Available Online at http://www.jart.ma

Journal of Atlantic Research and Technology

A computational study of the Diels-Alder reaction of PTAD as a dienophile leading to octahydropyridopyridazines.

Amine Rafik[a,b], Abdeljabbar Jaddi[a], Omar Fennane[a], Khalid Abbiche[a], Khadija Marakchi[a,*]

[a] *Laboratory of Spectroscopy, Molecular Modeling, Materials, Nanomaterials, Water and Environment, LS3MN2E/CERNE2D, Faculty of Sciences, Mohammed V University in Rabat, P.O. Box 1014, Rabat, Morocco.*
[b] *Departamento de Ciencias Integradas, Centro de Estudios Avanzados en Física, Matemática y Computación, Unidad Asociada GIFMAN, CSIC-UHU, Universidad de Huelva, Huelva, 21071, Spain.*

ARTICLE INFO

Article history:
Received 15th October, 2025
Received in revised form 18th December, 2025
Accepted 21st December, 2025
Available online 31th December, 2025

Keywords:
PTAD
Pyridopyridazine
Diels-Alder
DFT
Mechanism

ABSTRACT

PTAD is one of the most important dienophiles in Diels–Alder chemistry. One of its applications is in reactions with pyridine-based dienes to afford octahydropyridopyridazines. In this work we study the mechanism of the reaction of PTAD with a pyridine-based diene and explore the reaction using a differently substituted diene as well as in the environmentally friendly 2-Methyltetrahydrofuran solvent. The reaction paths are characterized in the gas phase, in dichloromethane and in 2-Methyltetrahydrofuran solvents, at the B3LYP/6-311G(d,p) level of theory, and the mechanism is studied using the Molecular Electron Density Theory. The results reproduce the available experimental work with reliable accuracy. It is shown that the reaction follows the standard asynchronous one-step mechanism. Moreover, it is shown that the reaction can be extended for the second diene and is feasible in the 2-Methyltetrahydrofuran solvent.

1. Introduction

Electron-poor azo compounds are exceptionally useful dienophiles in Diels–Alder chemistry as their strong electron-withdrawing substituents tend to facilitate rapid cycloaddition with electron-rich dienes under mild conditions [1,2]. This high reactivity enables efficient construction of nitrogen-containing ring systems in a single step, making these azo dienophiles valuable tools for synthesizing complex heterocycles, natural-product frameworks, and functionalized cycloadducts with excellent regio- and stereocontrol. Most notably, 4-phenyl-1,2,4-triazoline-3,5-dione (PTAD) is one of the most used dienophiles in Diels–Alder chemistry [3,4]. PTAD consists of a five-membered 1,2,4-triazoline ring bearing two carbonyl groups at the 3- and 5-positions and a phenyl substituent on the N-4 nitrogen. The three ring nitrogens are arranged as –N–N=C–, with the adjacent C(=O) units flanking the C=N moiety. The result is a highly electron-deficient heterocycle. One of the interesting applications of PTAD as a dienophile was reported in a reaction with a pyridine-based diene (A), with a sulfonyl group on the nitrogen atom, to afford an octahydropyridopyridazine cycloadduct [5]. The reaction proceeds readily producing the product with a high yield and short reaction time making it a convenient method to obtain octahydropyridopyridazine products. The reaction was carried out in a dichloromethane solvent under standard conditions. In here, we carry out a computational study of the mechanism. Furthermore, it has also been experimentally shown that a similar diene is accessible [6], here, we extend the reaction by employing this diene (denoted B) to afford an octahydropyridopyridazine functionalized with an alkene in the pyridine ring but involving a less bulky methyl group on the oxygen which can affect the observed π-diastereoselectivity in the reaction with Diene A. The feasibility of the reaction will be studied in dichlormethane solvent as well as the environmentally friendly solvent 2-Methyltetrahydrofuran (2-MeTHF) that has recently gained attention as a green solvent for Diels-Alder reactions [7,8]. The reaction pathways for the reaction of A with PTAD are depicted in Scheme 1 where we can see that due to the asymmetry of the π-plane of the diene, it is possible to perform the cycloaddition from two different faces of the plane, we refer to these faces by the labels *f1* and *f2*.

*Corresponding author.

E-mail address: k.marakchi@um5r.ac.ma

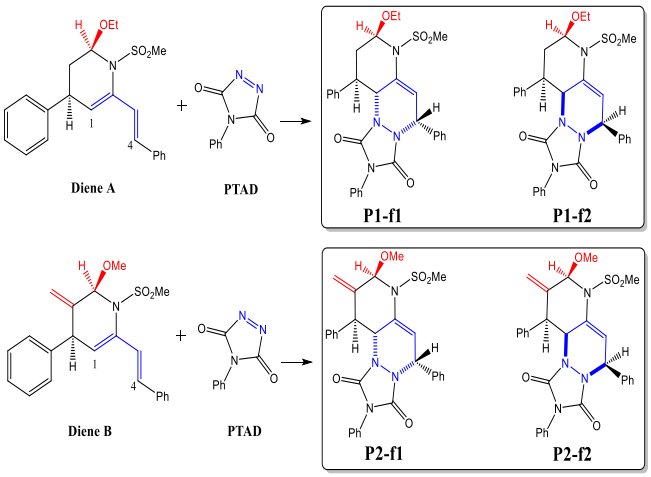

Scheme. 1. General scheme of the reaction of PTAD with dienes A and B.

Octahydropyridopyridazines refer to the hydrogenated pyridopyridazine derivatives, they exhibit a broad spectrum of biological activities including antitumor, antibacterial, analgesic, and diuretic properties, and function as selective phosphodiesterase inhibitors and GABA-A receptor ligands [9–11]. This work establishes a theoretical framework for studying the synthetic pathways to octahydropyridopyridazine, a highly relevant scaffold for drug agents, through DA reactions, in particular using green solvents like 2-MeTHF.

2. Computational Methods

The calculations are carried out at the B3LYP/6-311G(d,p) level of theory which has shown effective in modelling such system [12–18]. Frequency analysis was done to verify the stationary points and intrinsic reaction coordinate calculations to verify their connectivity through the reaction pathway. Solvation was accounted for implicitly using the self-coherent reaction field (SCRF) [19,20] with the polarizable continuum model (PCM). Conceptual Density Functional Theory is used to characterize the reactants according to the description provided in the reference [21–25]. The Electron Localization Function (ELF) and the Independent Gradient Model based on Hirshfeld partition of molecular density [26,27] are used to characterize the electronic characteristic and intermolecular interactions in the transition states, respectively. Gaussian 09 was used for the quantum chemistry calculations [28], Multiwfn 3.8 was used for IGMH calculations [29], and TopMod for the ELF ones [30]. GaussView 6.0 [31] and Visual Molecular Dynamics (VMD) package [32] were used for visualization.

3. Results and discussion

In the following sections we present and discuss the results of the study. Initially we characterize the reactants using CDFT and the ELF in section 3.1, then, in section 3.2 we discuss the thermodynamic and kinetic control of the reaction in CH_2Cl_2 and 2-MeTHF solvents in comparison to the gas phase reference. Finally, we discuss the reaction's mechanism from a topological point of view in section 3.3.

3.1. *Characterization of the reactants*

3.1.1. *Analysis of global CDFT indices of the reactants*

CDFT provides a means to systematically extracts fundamental chemical reactivity descriptors from the electron density of a molecular system. It is therefore a useful tool to characterize reactants. The Global CDFT indices are shown in Table 1.

Table 1
Global CDFT indices of PTAD and the dienes A and B. All indices are in units of eV

	HOMO	LUMO	μ	η	ω	N
PTAD	-7,27	-4,08	-5,68	3,19	5,05	2,14
Diene A	-6,53	-2,84	-4,69	3,69	2,98	2,88
Diene B	-6.08	-1.70	-3.89	4.38	1.73	3.33

The chemical potential can be interpreted as the tendency of an electron to escape, and in the context of CDFT, it serves as an approximate indicator of the expected polarity between reactants. PTAD exhibits a lower chemical potential than dienes A and B, suggesting that charge transfer occurs from the diene to the dienophile. The difference in chemical potentials is sufficient to promote a polar or moderately polar reaction. On the electrophilicity scale, both dienes qualify as strong electrophiles (ω>1.68 eV); however, PTAD (ω=5.05 eV) surpasses them, displaying super-electrophile behaviour that makes it the dominant electrophilic species. In terms of nucleophilicity, PTAD and A show a moderate level, whereas diene B is strongly nucleophilic (N>2.98 eV). Overall, these results indicate that PTAD acts as the electrophile, while the dienes serve as nucleophiles in the reactions under consideration.

3.1.2. *Analysis of local CDFT indices of the reactants*

Table 2
Local CDFT indices of PTAD and the dienes A and B.

	Site	P_k^+	P_k^-	ω_k	N_k
Diene A	**C1**	0.377686	0.282972	1.126	0.815
	C4	0.121874	0.163463	0.363	0.471
Diene B	**C1**	0.218310	0.365871	0.378	1.218
	C4	0.174134	0.079993	0.301	0.266
PTAD	**N1**	0.259831	0.003519	1.312	0.008
	N2	0.259839	0.00352	1.312	0.008
	C	0.110043	-0.022359	0.556	-0.05
	O	0.154441	0.053694	0.78	0.115

Table 2 reports results of Parr functions and the corresponding local CDFT indices, the local electrophilicity ω_k and local nucleophilicity N_k. The dienes A and B show relatively similar results with C1 being the most nucleophilic site ($N_k = 0.815/1.218$ for A/B). An electrophilic attack is therefore expected at the C1 carbon.

Considering that PTAD is symmetric, regiochemistry is omitted. However, PTAD contains both N=N and C=O double bonds which implies that the addition reaction can take place at any of these two bonds, we talk about a possible periselectivity. Looking at the computed local electrophilicities, we see that the N=N bond is by far the most electrophilic bond in comparison to the C=O bond ($\omega_k = 1.312\ vs\ \omega_k = 0.556/0.78$) implying that the reaction is completely periselective to the N=N bond in agreement with the numerous studies on the reactivity of PTAD.

3.1.3. *ELF analysis of the reactants*

The ELF is useful in the study of the evolution of electron density in chemical reactions. The standard procedure in employing the ELF method begins with the characterization of the isolated reactants. Fig. 1 shows the ELF attractor positions and their associated electronic populations.

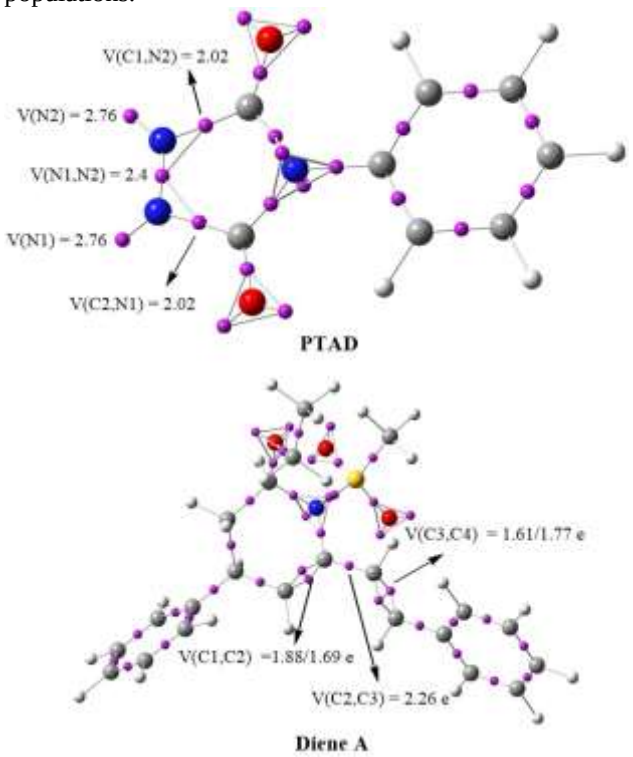

Fig. 1. ELF basin attractors and associated populations of PTAD and diene A, with electronic populations given in units of electron (e).

The ELF results show that PTAD undergoes significant delocalization of electrons in comparison to its standard Lewis notation. We see that the N=N bond of PTAD shows a monosynaptic basin with a population of 2.4 e much less than the expected 4 e for a double bond. The C=O bonds also show a monosynaptic basin integrating 2.57 e, slightly higher than that of N=N. Considering the powerful electrophilic nature of PTAD, we know that the reaction with A or B will involve the most electron-deficient bond, therefore we conclude that the reaction will occur at the N=N bond in agreement with the CDFT and experimental results for diene A.

3.2. Mechanistic analysis

3.2.1. Reaction Energy pathways

The reaction of PTAD with Diene A and Diene B is explored in the gas phase and in dichloromethane, in the case of diene B we also employ the 2-MeTHF solvent to explore the feasibility of this reaction in greener conditions. The results are reported in Fig. 2 and Fig. 3. We recall that the two explored pathways arise from the two possible approaches on the non-equivalent π-faces of the diene A. The computed relative energies and thermodynamics are given in Table 3 and a Gibbs free energy diagram is given in Fig. 2.

Table 3
The relative electronic energies ΔE (kcal.mol^{-1}), relative Gibbs free energies ΔG (kcal.mol^{-1}), relative enthalpies ΔH (kcal.mol^{-1}), and relative entropies ΔS (cal.mol^{-1}.K) of the products and TSs of the reaction of PTAD with A. All results are given at 25 °C.

	ΔE	ΔG	ΔH	ΔS
Gas phase				
P1-f1	-30.81	-9.49	-26.8	-58.05
P1-f2	-28.78	-8.37	-24.94	-55.58
TS1-f1	1.069	17.18	2.16	-50.4
TS1-f2	15.85	32.02	16.45	-52.23
Dichloromethane solvent				
P1-f1	-28.88	-8.07	-25.03	-56.89
P1-f2	-27.23	-5.75	-23.43	-59.31
TS1-f1	2.318	18.68	3.38	-51.31
TS1-f2	17.96	34.45	18.44	-53.72

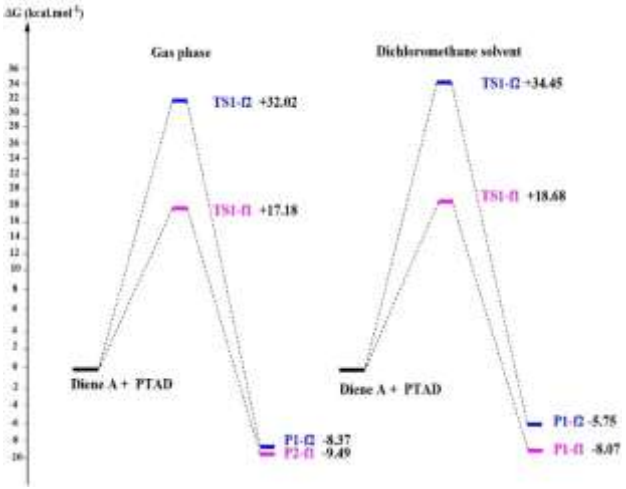

Fig. 2. Gibbs free energy profile of the reaction of PTAD with Diene **A** at room temperature, at the gas phase and in dichloromethane.

The gas phase and dichloromethane results show similar results; they indicate that the pathway leading to the P1-f1 product is both kinetically and thermodynamically the most stable. In dichloromethane, the barrier TS1-f1 barrier is 15.77 kcal.mol^{-1} lower than the TS1-f2 one. Moreover, the corresponding P1-f1 product is thermodynamically more stable by 2.33 kcal.mol^{-1} than P1-f2. These results indicate complete kinetic and thermodynamic selectivity and that an

approach from face 1 is the most affordable approach. The stability of TS1-f1 appear to primarily result from a much lower enthalpy (3.38 kcal.mol^{-1} in dichloromethane solvent) in comparison to that of TS1-f2 (18.44 kcal.mol^{-1} dichloromethane solvent), especially considering that both TSs have similar entropy losses.

Table 4
The relative electronic energies ΔE (kcal.mol^{-1}), relative Gibbs free energies ΔG (kcal.mol^{-1}), relative enthalpies ΔH (kcal.mol^{-1}), and relative entropies ΔS (cal.mol^{-1}.K) of the products and TSs of the reaction of PTAD with ***B***. All results are given at 25 °C.

	ΔE	ΔG	ΔH	ΔS
Gas phase				
P2-f1	-27.25	-6.87	-23.53	-55.87
P2-f2	-26.21	-5.51	-22.45	-56.82
TS2-f1	0.76	16.74	1.69	-50.47
TS2-f2	17.946	32.59	18.35	-47.77
Dichloromethane solvent				
P2-f1	-26.99	-6.27	-23.18	-56.69
P2-f2	-25.69	-4.33	-21.84	-58.72
TS2-f1	1.39	18.23	2.36	-53.2
TS2-f2	18.76	35.14	19.22	-53.39
2-MeTHF solvent				
P2-f1	-30.16	-6.06	-23.11	-57.21
P2-f2	-28.93	-4.36	-21.84	-58.64
TS2-f1	-1.80	18.18	2.40	-52.94
TS2-f2	15.51	34.96	19.21	-52.81

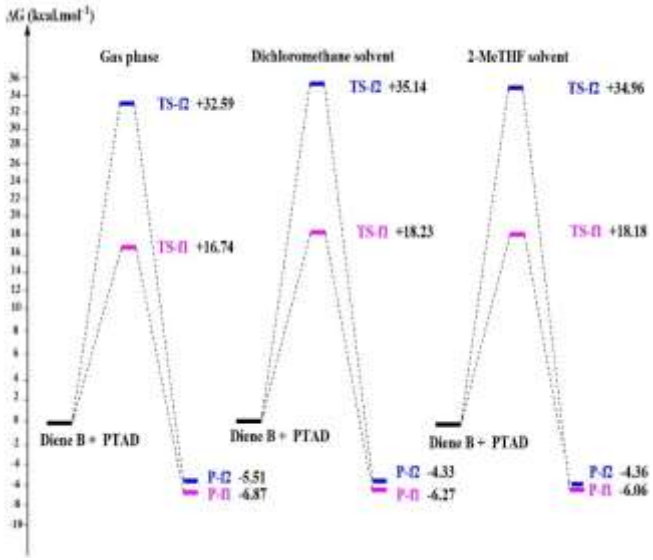

Fig. 3. Gibbs free energy profile of the reaction of PTAD with B at room temperature, in the gas phase, in dichloromethane and in 2-MeTHF.

The computed relative energies and thermodynamics for the reaction of PTAD and B are given in Table 4 and a Gibbs free energy diagram is given in Fig. 3. The reaction of PTAD with Diene *B* shows similar results to the previous one with Diene A. The approach f1 is by far the most stable both from the kinetic and thermodynamic perspectives in all environments. The TS energy of TS2-f1 is 16.74, 18.23 and 18.18 kcal.mol-1, which is 15.85, 16.91, and 16.77 kcal.mol^{-1} lower than that of TS2-f2. The cycloadducts are exergonic (ΔG = -6.87 kcal.mol^{-1} and -5.51 kcal.mol^{-1} in the gas phase) and entropy changes are negative reflecting increased order in both products. The products show less separation than the TSs but the favourability of the P2-f1 cycloadduct remains where it is 1.36-1.94 kcal.mol^{-1} more stable than the P2-f2. Overall, solvent effects slightly raise all barrier heights compared to the gas phase, with dichloromethane and 2-MeTHF producing similar ΔG. It is worthy to note that the 2-MeTHF solvent shows significant larger electronic stabilization (-1.80 kcal.mol-1) in comparison to the dichloromethane solvent, which solidifies the position of 2-MeTHF as a reliable alternative for the hazardous dichloromethane solvent.

3.2.2. Geometric analysis

The geometry of the most stable TS from the reaction of PTAD with Diene A and Diene B are depicted in Fig. 4 and Wiberg bond indices are shown in Table 5.

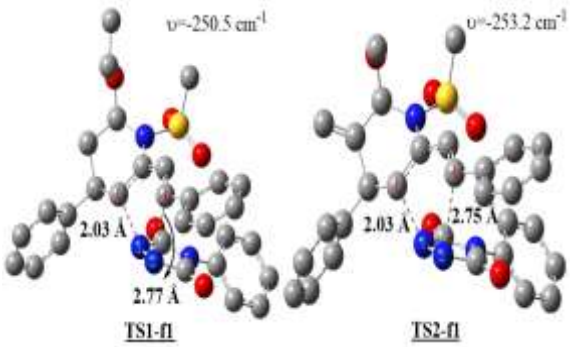

Fig. 4. Geometry of TS1-f1 and TS2-f1 from the reactions of PTAD with dienes A and B, respectively.

The transition states TS1-f1 and TS2-f1 exhibit similar geometries. Both have a geometry in which the PTAD fragment adopts an endo-like position where its phenyl substituent is at a close distance to the sulfonyl substituent on the dienes fragment. We would expect that these geometries allow the oxygens from the SO_2CH_3 group to interact with the phenyl group of PTAD and this will be investigated later in the IGM analysis section. With respect to the new σ bonds, we observe in both TSs what appears to be an asynchronous bond formation due to the large difference between the distances C1-N1 and C2-N2. Indeed, the distance C1-N1 is 2.03 Å in both TS1-f1 and TS2-f1, while the distance C2-N2 is 2.77 and 2.75 Å in TS1-f1 and TS2-f1, respectively. A better evaluation of the asynchronicity is possible through analysis of the Wiberg bond indices.

In the reaction of PTAD with A, particularly in TS1-f1, the reaction favors early formation of C1–N1, while C4–N2 lags far behind. C4–N2 is only about 10% formed while C1–N1 is 41% formed in the TS. In contrast, in TS1-f2, it is C4–N2 that is much further along than C1–N1, advancing it by about 28%. Moving to the reaction of PTAD with B, we see that the results mirror those of the

reaction with diene A, where C1–N1 formation is ahead for the f1 TS while C4-N2 is ahead for the f2 TS. In general, the early bond in each case is roughly 40–55% formed, while the delayed bond is 10–25% formed in the TS. This indicates asynchronous bond formation, i.e., an asynchronous DA mechanism.

Table 5
Wiberg bond indices and bond formation percentages at transition structures.

	TS1-f1	**P1-f1**	**TS1-f2**	**P1-f2**
C1-N1	0.3777	0.9149	0.2281	0.9182
%	41.28		24.84	
C4-N2	0.0942	0.9295	0.4906	0.9234
%	10.13		53.13	
	TS2-f1	**P2-f1**	**TS2-f2**	**P2-f2**
C1-N1	0.3812	0.928	0.1651	0.9218
%	41.08		17.91	
C4-N2	0.0973	0.8918	0.5073	0.9203
%	10.91		55.12	

3.2.3. Global Electron Density analysis

The Global Electron Density Transfer (GEDT) is a quantitative index derived from the analysis of atomic charges, that measures the net flow of electron density between interacting fragments in a transition state. A higher GEDT value indicates greater electron transfer, providing a simple way to assess the polar character and driving forces of a reaction. The Global Electron Density Transfer (GEDT) values for the TSs associated with both reactions are shown in Table 6. Following the formalism of the GEDT, the positive values imply a density transfer from the dienes A or B to PTAD, in other words, a forward electron density flux (FEDF) process in accordance with earlier results from the chemical potential.

Table 6
Transition state global electron density transfer (in units of e) in the gas phase for the reactions of PTAD with A and B.

	TS1-f1	**TS1-f2**	**TS2-f1**	**TS2-f2**
GEDT	0.32	0.42	0.32	0.39

The GEDT values for the f1 and f2 TSs for both reactions are 0.32, 0.42, 0.32, and 0.39 e, respectively. Clearly, all TSs are highly polar where reactions are commonly considered polar when their GEDT is higher than 0.20 e. These finding indicate a polar DA reaction. It is well known that higher GEDT correlates with lower barriers in strongly polar reactions [33], however, the considered reactions disagree with this idea. Indeed, the more stable *f1* TSs from both reactions in fact show a lower GEDT than the higher barrier *f2* TSs.

3.2.4. IGM analysis

The Independent Gradient Model and its variants like the IGMH, analyse and visualize non-covalent interactions and bonding characteristics in molecules, including transition states states of chemical reactions. Instead of just looking at bonds directly, the IGM examines how the cloud of electrons around atoms changes when they come close together. In particular, it is based on analysing the gradient of the electron density. By highlighting regions where the density gradient is reduced, IGM helps identify areas of interaction, such as stabilizing or destabilizing forces. Fig. 5 depicts the results of the IGMH calculation on the transition states from the reactions of PTAD with both dienes. In the reaction of PTAD with diene A, we see that TS1-f1 presents a larger blue surface in the region of the C1-N1 forming bond than that in the C4-N2 region indicating a highly asynchronous process. The same cannot be said about TS1-f2 where the asynchronicity is less pronounce and notably it is the C4-N2 that appears to experience the strongest attraction in this TS. Additionally, TS1-f1 also presents two small green contours, one involves the oxygen from the carbonyl of PTAD and an axial hydrogen from the pyridine ring. The second contour involves an oxygen from the sulfonyl group of the Diene A and a hydrogen from the benzene substituent on PTAD. TS1-f2 shows neither of these interactions and therefore they could be responsible partially for stabilizing the *f1* approach.

In the reaction of PTAD with diene B, we see that it is TS2-f2 that shows a highly asymmetric attraction pattern in the bonding sites. In particular, the C4-N2 bonding region shows a strong blue map while the C1-N1 region shows none. In comparison, the TS from the f1 face, shows a blue zone in the C1-N1 region and a cyan-coloured zone in the C4-N2 region. It is notable that the alkene group on the pyridine ring appears to force the phenyl group to adopt an orientation such that its plane is perpendicular to the plan formed by the pyridine ring. This orientation was not observed in TS1-f2 (i.e., the reaction of PTAD with diene A) and it leads to shortening the distance between the phenyl hydrogens and the oxygen from the carbonyl group of PTAD. Consequently, in TS2-f2, unlike TS1-f2, we notice a green zone between the oxygen from PTAD and one of the phenyl hydrogens.

3.2.5. ELF analysis

In a chemical reaction, electrons shift around as old bonds start to break and new ones begin to form. The ELF creates a kind of map that shows where electrons are tightly grouped or more spread out, giving insight into how old bonds are breaking and new ones are forming. We pick the TS1-f1 and TS1-f2 from the reaction of PTAD and diene A as an example to elucidate the evolution of the electron populations of the two reacting fragments in the transition state. The results are shown in Fig. 6.

The results for both TS1-f1 show that the diene's double bonds C1-C2 and C3-C4 are undergoing an impoverishment of electron density where the total electron population in both bonds has dropped to 3.07 and 3.12 e from the idealistic 4 e in each bond, respectively. A similar finding is observed in TS1-f2 where the C1-C2 and C3-C4 populations have dropped to 2.98 and 2.67 e, respectively.

In contrast, the C2-C3 bond gains in population where the attractor basin integrates 2.63 and 2.82 e in TS1-f1 and TS1-f2 respectively. This synergy reflects the change associated with the breaking of the original double bonds and creating of the new C2=C3 one. Moreover, in the case of TS1-f1, the charge transfer appears to be ongoing from the side of C1 atom in the diene (to the N atom in the PTAD), this is shown by the decrease in the population of the C1-C2 bond by 0.5 e in going from the reactant (3.57 e) to TS1-f1 (3.07 e) while C3-C4 only decreases by 0.26 e. Conversely, it occurs from the side of the C4 atom in the diene in TS1-f2 and this is shown by a pronounce drop in the population of C3-C4 bond from 3.38 e in the reactant to 2.67 e in TS1-f2, decreasing by 0.71 e while it only decreases by 0.59 e in the C1-C2 bond. A distinct feature of TS1-f2 is that the carbon C4 shows a monosynaptic basin V(C4) with a small population of 0.12 e. This small basin is a prime spot for new bond formation and indicates the regrouping of electron density in the bonding region in preparation to form the new C4-N2 sigma bond. In general, the TSs do not show any distinct features of unfamiliar mechanism, in fact, the findings indicate that reaction paths follow an asynchronous one-step mechanism.

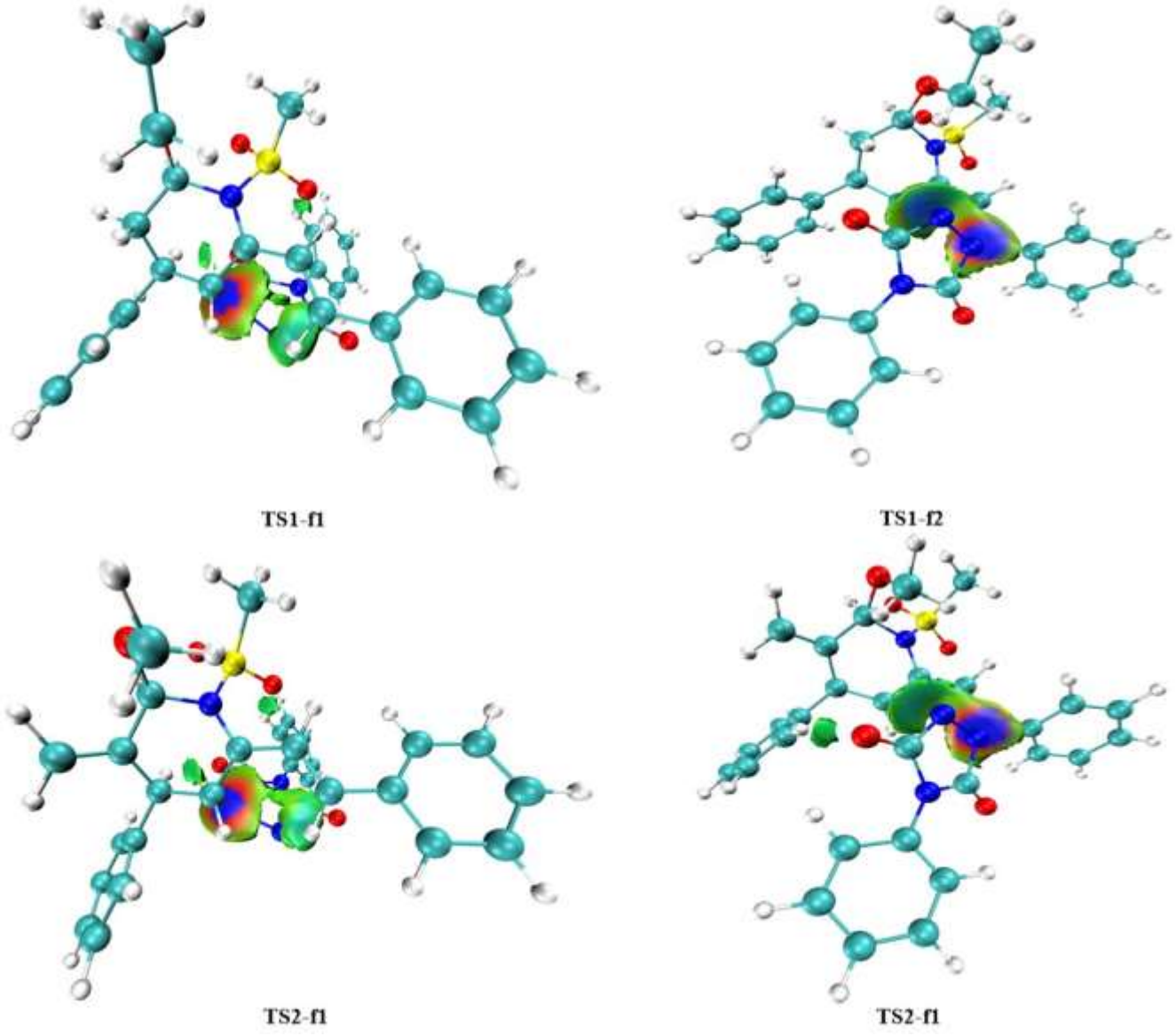

Fig. 5. The IGM's Sign(λ2)ρ coloured isosurfaces of δg^{inter} = 0.008 a.u for of for all TSs in both reactions of PTAD with Diene A (top) and Diene B (Bottom).

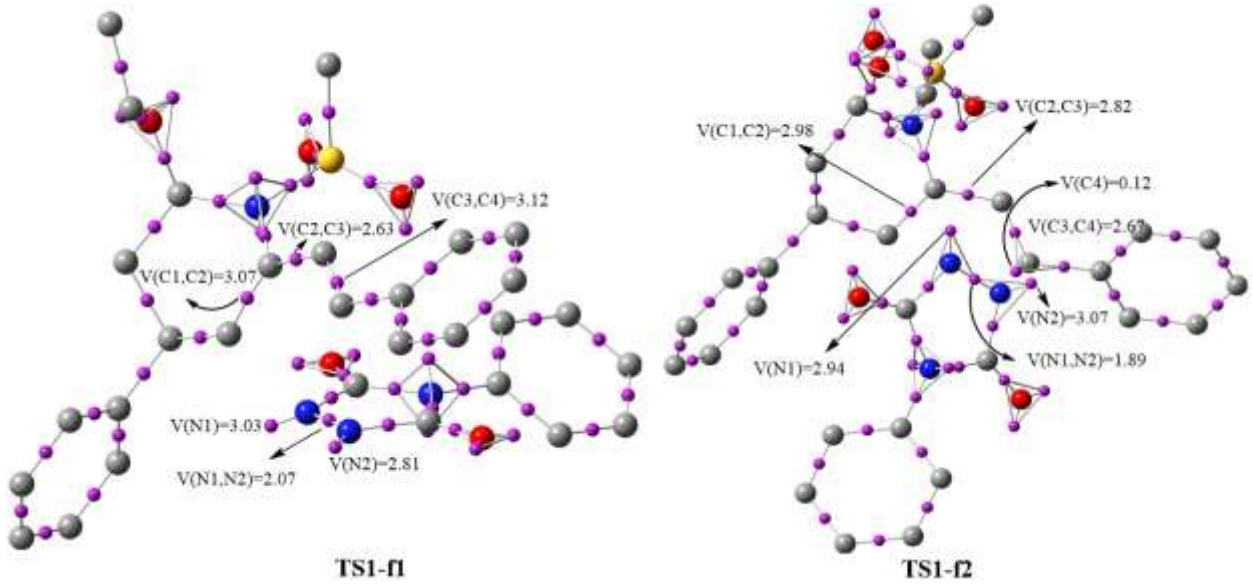

Fig. 6. ELF basin attractor positions given with population values for the most relevant sites for the stable TSs from the reaction of PTAD with diene A.

Conclusion

The reaction of PTAD with two pyridine-based dienes leading to hydrogenated pyridopyridazines is explored with a theoretical approach based on the molecular electron density theory with the computations carried out at the B3LYP/6-311G(d,p) level of theory. The facial selectivity observed experimentally is reproduced at the level of the employed models and it is shown that the *f1* approach is roughly twice as kinetically stable as the corresponding *f2* approach. The mechanism of reactions is elucidated to be a one-step asynchronous mechanism. Furthermore, the reaction is extended with a different diene and it is shown that despite some small mechanistic differences, the overall reaction is similar to the experimental one, moreover, it is also shown that the reaction can be carried out in the green solvent 2-Methyltetrahydrofuran. The studied reaction route to octahydropyridopyridazines is a highly efficient method that can afford a variety of substituted cycloadducts, and adopting the 2-Methyltetrahydrofuran solvent should make the procedure more environmentally friendly.

Acknowledgement (optional)

The authors acknowledge the Moroccan Association of Theoretical Chemists for providing the computational programs.

Conflicts of interest statement

The authors declare no competing financial interest.

References

[1] W. Shi, J. Sun, C.-G. Yan, Aza-Diels-Alder reaction of both electron-deficient azoalkenes with electron-deficient 3-phencaylideneoxindoles and 3-aryliminooxindol-2-ones, Green Synthesis and Catalysis 2 (2021) 362–366.

[2] S.M.M. Lopes, A.L. Cardoso, A. Lemos, T.M.V.D. Pinho e Melo, Recent Advances in the Chemistry of Conjugated Nitrosoalkenes and Azoalkenes, Chem. Rev. 118 (2018) 11324–11352.

[3] M.P. Johnson, C.J. Moody, Azo dienophiles. Diels–Alder reactions of 4-phenyl-1,2,4-triazole-3,5-dione and 5-phenylpyrazol-3-one with functionalised dienes, J. Chem. Soc., Perkin Trans. 1 (1985) 71–74.

[4] T.C. Celius, Fast Hetero-Diels−Alder Reactions Using 4-Phenyl-1,2,4-triazoline-3,5-dione (PTAD) as the Dienophile, J. Chem. Educ. 87 (2010) 1236–1237.

[5] S. Kobayashi, T. Furuya, T. Otani, T. Saito, A diene-transmissive Diels–Alder reaction involving inverse electron-demand hetero-Diels–Alder cycloaddition of cross-conjugated azatrienes, Tetrahedron Letters 49 (2008) 4513–4515.

[6] S. Kobayashi, T. Furuya, T. Otani, T. Saito, A novel and facile stereocontrolled synthetic method for polyhydro-quinolines and pyridopyridazines via a diene-transmissive Diels–Alder reaction involving inverse electron-demand hetero Diels–Alder cycloaddition of cross-conjugated azatrienes, Tetrahedron 64 (2008) 9705–9716.

[7] V. Antonucci, J. Coleman, J.B. Ferry, N. Johnson, M. Mathe, J.P. Scott, J. Xu, Toxicological Assessment of 2-Methyltetrahydrofuran and Cyclopentyl Methyl Ether in Support of Their Use in Pharmaceutical Chemical Process Development, Org. Process Res. Dev. 15 (2011) 939–941.

[8] V. Pace, P. Hoyos, L. Castoldi, P. Domínguez de María, A.R. Alcántara, 2-Methyltetrahydrofuran (2-MeTHF): A Biomass-Derived Solvent with Broad Application in Organic Chemistry, ChemSusChem 5 (2012) 1369–1379.

[9] M.A. Ibrahim, A.H. Elmenoufy, M. Elagawany, M.M. Ghoneim, A. Moawad, "Pyridopyridazine": A Versatile Nucleus in Pharmaceutical Field, Journal of Biosciences and Medicines 3 (2015) 59–66.

[10] A. Wojcicka, A. Nowicka-Zuchowska, Synthesis and Biological Activity of Pyridopyridazine Derivatives: A Mini Review, Mini-Reviews in Organic Chemistry 16 (2019) 3–11.

[11] N.A. Meanwell, The pyridazine heterocycle in molecular recognition and drug discovery, Med Chem Res 32 (2023) 1853–1921.

[12] A. Jaddi, A. Rafik, S. Sebbahi, M. Salah, K. Marakchi, Mechanistic insights and antifungal assessment of (3+2) cycloaddition products of 2-diazopropane and 5-hydroxy-3-

methyl-1,5-dihydropyrrol-2-one derivatives, 10.5267/j.Ccl 14 (2025) 547–558.
[13] A. Rafik, A. Jaddi, M. Salah, N. Komiha, M. Carvajal, K. Marakchi, Insights into the mechanism, selectivity, and substituent effects in the Diels-Alder reaction of azatrienes with electron-rich dienophiles: An MEDT study, Journal of Molecular Graphics and Modelling 132 (2024) 108819.
[14] A. Rafik, H. El Hadki, A. Jaddi, N. Komiha, O.K. Kabbaj, N. Acharjee, M. Salah, M. Azam, K. Marakchi, A new investigation into the regioselectivity and stereoselectivity of the reaction between di-methyl nitrone and fluorinated alkenes: DFT, independent gradient model, and molecular docking, Computational and Theoretical Chemistry 1234 (2024) 114511.
[15] M. Ríos-Gutiérrez, F. Falcioni, L. R. Domingo, P.L. A. Popelier, A combined BET and IQA–REG study of the activation energy of non-polar zw-type [3+2] cycloaddition reactions, Physical Chemistry Chemical Physics 25 (2023) 10853–10865.
[16] L.R. Domingo, K. Kula, M. Ríos-Gutiérrez, R. Jasiński, Understanding the Participation of Fluorinated Azomethine Ylides in Carbenoid-Type [3 + 2] Cycloaddition Reactions with Ynal Systems: A Molecular Electron Density Theory Study, J. Org. Chem. 86 (2021) 12644–12653.
[17] K. Abbiche, N. Acharjee, M. Salah, M. Hilali, A. Laknifli, N. Komiha, K. Marakchi, Unveiling the mechanism and selectivity of [3+2] cycloaddition reactions of benzonitrile oxide to ethyl trans-cinnamate, ethyl crotonate and trans-2-penten-1-ol through DFT analysis, J Mol Model 26 (2020) 279.
[18] M. Salah, A. Zeroual, S. Jorio, H. El hadki, O.K. Kabbaj, K. Marakchi, N. Komiha, Theoretical study of the 1,3-DC reaction between fluorinated alkynes and azides: Reactivity indices, transition structures, IGM and ELF analysis, Journal of Molecular Graphics and Modelling 94 (2020) 107458.
[19] M. Cossi, V. Barone, R. Cammi, J. Tomasi, Ab initio study of solvated molecules: a new implementation of the polarizable continuum model, Chemical Physics Letters 255 (1996) 327–335.
[20] V. Barone, M. Cossi, J. Tomasi, Geometry optimization of molecular structures in solution by the polarizable continuum model, J. Comput. Chem. 19 (1998) 404–417.
[21] R.G. Pearson, The electronic chemical potential and chemical hardness, Journal of Molecular Structure: THEOCHEM 255 (1992) 261–270.
[22] L. Domingo, M. Ríos-Gutiérrez, P. Pérez, Applications of the Conceptual Density Functional Theory Indices to Organic Chemistry Reactivity, Molecules 21 (2016) 748.
[23] L.R. Domingo, P. Pérez, The nucleophilicity N index in organic chemistry, Org. Biomol. Chem. 9 (2011) 7168.
[24] L.R. Domingo, P. Pérez, J.A. Sáez, Understanding the local reactivity in polar organic reactions through electrophilic and nucleophilic Parr functions, RSC Adv. 3 (2013) 1486–1494.
[25] E. Chamorro, P. Pérez, L.R. Domingo, On the nature of Parr functions to predict the most reactive sites along organic polar reactions, Chemical Physics Letters 582 (2013) 141–143.
[26] B. Silvi, A. Savin, Classification of chemical bonds based on topological analysis of electron localization functions, Nature 371 (1994) 683–686.
[27] T. Lu, Q. Chen, Independent gradient model based on Hirshfeld partition: A new method for visual study of interactions in chemical systems, Journal of Computational Chemistry 43 (2022) 539–555.
[28] M.J. Frisch, G.W. Trucks, H.B. Schlegel, G.E. Scuseria, M.A. Robb, J.R. Cheeseman, G. Scalmani, V. Barone, B. Mennucci, G.A. Petersson, H. Nakatsuji, M. Caricato, X. Li, H.P. Hratchian, A.F. Izmaylov, J. Bloino, G. Zheng, J.L. Sonnenberg, M. Hada, M. Ehara, T. Vreven, J.A. Montgomery, R.L. Martin, J.E. Peralta, J.J. Heyd, E. Brothers, F. Ogliaro, M. Bearpark, K.N. Kudin, V.N. Staroverov, R. Kobayashi, J. Normand, A. Rendell, R. Gomperts, V.G. Zakrzewski, K. Toyota, R. Fukuda, J. Hasegawa, M. Ishida, T. Nakajima, Y. Honda, O. Kitao, H. Nakai, Gaussian 09, (n.d.).
[29] T. Lu, F. Chen, Multiwfn: A multifunctional wavefunction analyzer, J Comput Chem 33 (2012) 580–592.
[30] S. Noury, X. Krokidis, F. Fuster, B. Silvi, Computational tools for the electron localization function topological analysis, Computers & Chemistry 23 (1999) 597–604.
[31] R. Dennington, T.A. Keith, J.M. Millam, GaussView, Version 6.1, (2016).
[32] W. Humphrey, A. Dalke, K. Schulten, VMD: Visual molecular dynamics, Journal of Molecular Graphics 14 (1996) 33–38.
[33] L.R. Domingo, M. Ríos-Gutiérrez, P. Pérez, How does the global electron density transfer diminish activation energies in polar cycloaddition reactions? A Molecular Electron Density Theory study, Tetrahedron 73 (2017) 1718–1724.